

Algebraic Bethe Circuits

Alejandro Sopena,^{1,*} Max Hunter Gordon,^{1,2,*} Diego García-Martín,^{3,1} Germán Sierra,¹ and Esperanza López¹

¹*Instituto de Física Teórica, UAM/CSIC, Universidad Autónoma de Madrid, Madrid, Spain*

²*Theoretical Division, Los Alamos National Laboratory, Los Alamos, NM 87545, USA*

³*Barcelona Supercomputing Center, Barcelona, Spain*

The Algebraic Bethe Ansatz (ABA) is a highly successful analytical method used to exactly solve several physical models in both statistical mechanics and condensed-matter physics. Here we bring the ABA to unitary form, for its direct implementation on a quantum computer. This is achieved by distilling the non-unitary R matrices that make up the ABA into unitaries using the QR decomposition. Our algorithm is deterministic and works for both real and complex roots of the Bethe equations. We illustrate our method in the spin- $\frac{1}{2}$ XX and XXZ models. We show that using this approach one can efficiently prepare eigenstates of the XX model on a quantum computer with quantum resources that match previous state-of-the-art approaches. We run numerical simulations, preparing eigenstates of the XXZ model for systems of up to 24 qubits and 12 magnons. Furthermore, we run small-scale error-mitigated implementations on the IBM quantum computers, including the preparation of the ground state for the XX and XXZ models in 4 sites. Finally, we derive a new form of the Yang-Baxter equation using unitary matrices, and also verify it on a quantum computer.

I. INTRODUCTION

One of the most widely-recognized applications of quantum computing is the efficient simulation of many-body quantum systems [1]. Simulating such systems using classical devices generally requires computational resources that scale exponentially with the size of the system. Quantum computers on the other hand are naturally suited to this task, being themselves quantum systems and hence overcoming the classical exponential scaling. In this context, preparing Bethe Ansatz (BA) eigenstates on a quantum computer is attracting increasing attention [2–5].

The BA is an extremely successful classical method for exactly solving one-dimensional (1D) quantum models, *e.g.* the Heisenberg, Hubbard or Kondo models [6–9]. It reduces the difficult problem of diagonalizing the Hamiltonian to finding the solutions of a set of algebraic equations. In many cases, it is possible to numerically solve these equations, which in turn allows one to calculate the eigenvalues and the eigenvectors of the system of interest. These quantities are computed differently depending on whether the coordinate Bethe Ansatz (CBA) or the Algebraic Bethe Ansatz (ABA) is used [9]. In both cases, the eigenstates are represented as complex mathematical expressions. As a result, this method does not allow direct access to some physical quantities, such as high-order and long-range correlation functions, which have proved challenging to compute both analytically and numerically [10, and references therein]. This motivates the construction of such states directly on a quantum computer. Once the eigenstates are experimentally available, all the correlation functions can be readily computed from measurements. Furthermore, these states can be used to initialise other quantum algorithms or benchmark quantum hardware.

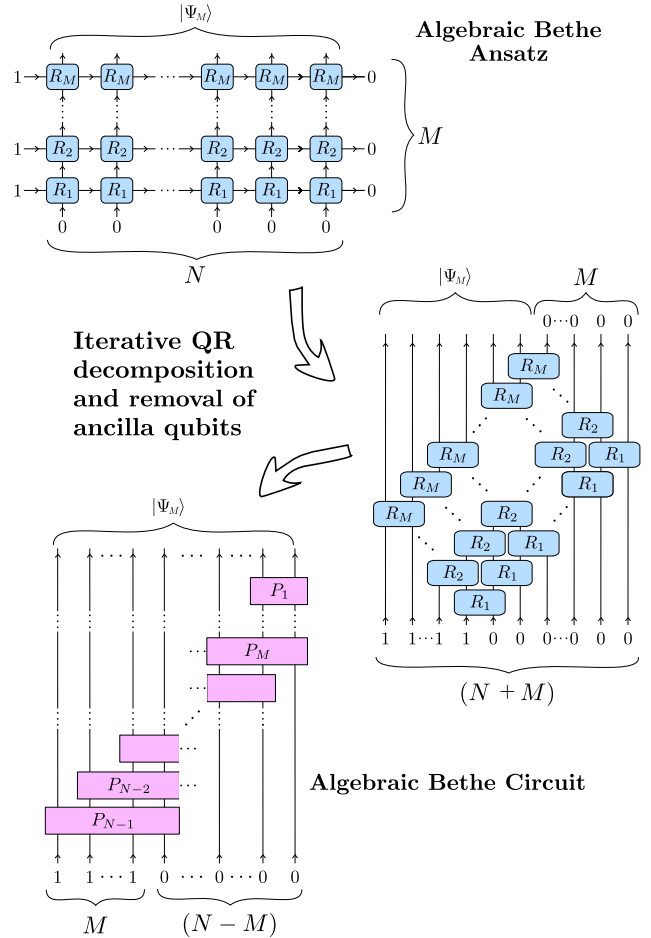


FIG. 1. A Bethe ansatz eigenstate $|\Psi_M\rangle$ for M magnons in N sites, converted into a quantum circuit of N qubits by computing iterative QR decompositions and removing the ancilla qubits, as explained in the main text. The R_j are the tensors defined in (7) that satisfy the YB equation, and the P_k are unitary matrices of dimension $2^{n+1} \times 2^{n+1}$ with $n = \min(k, M)$. These matrices need to be compiled to quantum gates before implementation on a quantum computer.

* The first two authors contributed equally.

To this end, a quantum algorithm for the preparation of the eigenstates of the spin- $\frac{1}{2}$ XXZ model in 1D was introduced in Refs. [3, 4], based on the CBA. This algorithm is probabilistic and works for real-valued solutions of the Bethe equations. Its circuit depth is polynomial in both the system size and number of magnons, or down spins. However, it was recently shown [5] that the success probability of obtaining the desired eigenstate upon measurement of the ancillary qubits decreases super-exponentially with the number of magnons for large chains. The use of a variational approach for the preparation of integrable-system eigenstates, which does not rely on knowledge coming from the BA, has also been considered [11–14]. Variational quantum algorithms are known to suffer from exponentially-vanishing gradients [15, 16]. This problem is certain to appear when the number of magnons scales with the system size [17]. Moreover, even when the number of magnons is fixed this issue is likely to persist for large chains due to the effect of noise [18].

In this paper, we present a quantum algorithm based on the ABA for the preparation of BA eigenstates. Contrary to [3], it also works for complex solutions of the Bethe equations. The main difficulty encountered when directly trying to convert the ABA into a quantum circuit is that the matrices R are not unitary. Besides, the circuit translation of the ABA requires the use of ancillas which need to be projected onto the $|0\dots 0\rangle$ state at the end of the computation. This would yield a probabilistic algorithm should a direct translation be employed. We circumvent both of these issues by iteratively computing the QR decomposition [19] of the non-unitary matrices appearing in the ABA. This then allows us to obtain the desired eigenstate as the output of a quantum circuit with no ancillary qubits, which we refer to as an Algebraic Bethe Circuit (ABC). The process is sketched in Fig. 1. We note that quantum circuits based on unitary R matrices were explored to compute infinite temperature correlation functions in [20].

We focus on the paradigmatic 1D anti-ferromagnetic spin- $\frac{1}{2}$ XXZ model with periodic boundary conditions for the concrete analysis. The complexity of calculating the ABC unitaries scales linearly in the number of sites (qubits), but exponentially in general with the number of magnons. There is the additional complexity of compiling the calculated unitaries, which may also scale exponentially. This means that our algorithm is in general only applicable to a small number of magnons. In spite of that, it allows for the preparation of states on near-term quantum hardware that have been challenging before. Besides, we find that its application on the XX model is efficient. This model is free, describing spinless fermions via a Jordan-Wigner transformation. Here, the ABCs match the performance of the state-of-the-art algorithms for the preparation of fermionic states [21–23], both in the number of gates necessary and the circuit depth.

From a theoretical standpoint, the ABCs offer an alternative approach towards finding exact circuits for

quantum integrable many-body systems [24, 25]. Along these lines, we derive a novel version of the Yang-Baxter equation in terms of unitary matrices which can be tested on quantum hardware. Interestingly, the BA can be interpreted as a Matrix Product State (MPS) [26–28]. Our algorithm for the distillation of unitaries from the ABA appears closely related to the transformation of an MPS into canonical form [29], which in turn has a direct translation to a quantum circuit. Hence our method to obtain the ABCs should also prove relevant for the circuit implementation of general MPS with low bond dimension. Let us mention that several works have considered the implementation of tensor-network states on a quantum computer [30–35].

The paper is structured as follows. In Section II we briefly introduce the ABA. Section III contains a detailed explanation of its transformation into a quantum circuit, together with a preliminary discussion on the decomposition of the ABC unitaries in terms of elementary quantum gates. The unitary version of the YB equation is discussed in Section IV. Section V contains numerical simulations up to 12 magnons and small-scale error-mitigated implementations of the ABCs on quantum hardware. In particular, we prepare plane wave states in 8 sites and implement the ground state of the XX and XXZ models in 4 sites using the IBM cloud computers. Section V also includes a test of the YB equation on quantum hardware. Finally, we conclude in Section VI with a discussion of our results. Several technical details are confined to Appendices.

II. THE ALGEBRAIC BETHE ANSATZ

The Algebraic Bethe Ansatz [7–9] is a powerful classical technique to solve one-dimensional quantum integrable vertex models. These models fulfill the so-called Yang-Baxter (YB) equation [36], and are characterised by an extensive set of conserved quantities. They have been greatly studied over the last century in the context of quantum many-body physics [37, 38].

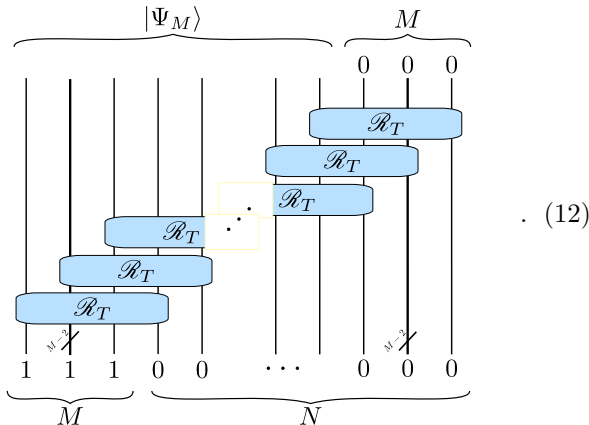
The ABA can be used to calculate the exact eigen-spectrum of a large class of Hamiltonians in terms of a matrix R that satisfies the YB equation. Among these models, a prominent example is the 1D spin- $\frac{1}{2}$ anti-ferromagnetic XXZ Hamiltonian with periodic boundary conditions,

$$H_{\text{XXZ}} = \sum_{j=1}^N (\sigma_j^x \sigma_{j+1}^x + \sigma_j^y \sigma_{j+1}^y + \Delta \sigma_j^z \sigma_{j+1}^z), \quad (1)$$

where $\{\sigma_j^x, \sigma_j^y, \sigma_j^z\}$ are the Pauli matrices acting on the j -th spin, and $\sigma_{N+1} \equiv \sigma_1$. The parameter Δ introduces an anisotropy in the chain. When $\Delta = 1$ we recover the isotropic anti-ferromagnetic Heisenberg spin chain, which has $SU(2)$ symmetry. For other values of Δ , only a $U(1)$ symmetry is present. In order to use the R matrix to construct the eigenstates of the Hamiltonian, a set of algebraic equations needs to be solved. These are

where $R_j \equiv R(\lambda_j)$. The problem encountered when directly trying to transform this cell into a quantum gate is that the matrices R are in general not unitary (see Appendix A).

To stress the crucial difference between unitary and non-unitary matrices, we shall use rounded-corner rectangles for the latter. The complete ABA network can be recast in terms of the \mathcal{R}_T cells as



The M rightmost qubits, both at the input and output, are in the fixed state $|0\rangle$. They can be considered ancillary qubits. Keeping them in the final quantum circuit we are seeking would result in a probabilistic algorithm. A severe reduction of the success probability with increasing M is to be expected due to the curse of dimensionality. The probabilistic quantum algorithm based on the CBA proposed in [3] was recently shown to suffer from a similar problem [5].

Both the conversion of (12) into a quantum circuit and the removal of the ancillary qubits can be addressed by utilising the QR decomposition as our main tool. To be more precise, any $m \times n$ matrix can be written as the product of two matrices $Q \cdot R$. When $m \leq n$, Q is a $m \times m$ unitary and R an $m \times n$ rectangular matrix with vanishing entries below the main diagonal. When $m > n$, Q is a $m \times n$ isometry (*i.e.* $Q^\dagger Q = \mathbb{1}_n$) and R an $n \times n$ upper triangular matrix. We note that the QR decomposition was previously used in the derivation of efficient quantum circuits in [21–23, 41].

We start our protocol at the top-rightmost basic cell. All the information in this cell can be encoded in a 2×2^M matrix defined by

Working directly with G_0 allows us to eliminate the rightmost ancillary qubit. The matrix G_0 can then be absorbed into the second \mathcal{R}_T cell. This defines a 4×2^M matrix which renders the second rightmost qubit unnecessary. We apply now the QR decomposition to this

matrix, obtaining

$$(\mathbb{1} \otimes G_0)\mathcal{R}_T|0\rangle = P_1 G_1, \quad (14)$$

or graphically

We have distilled the first gate of the deterministic quantum circuit for the construction of Bethe eigenstates, the two-qubit unitary P_1 . The non-unitary remainder G_1 is then absorbed into the next basic cell and the QR decomposition is computed again for the new non-unitary matrix. As before, one more ancillary qubit is eliminated. This process is iterated. At each step a unitary gate P_k acting on $k+1$ qubits is obtained. After $M-1$ iterations all ancillary qubits have been removed and the M top-right basic cells have been substituted by the circuit

For $k \geq M$ each new step is described by the recursion relation

$$(\mathbb{1} \otimes G_{k-1})\mathcal{R}_T|0\rangle = (P_k|0\rangle)G_k, \quad (17)$$

or equivalently

The LHS defines a $2^{M+1} \times 2^M$ matrix. The matrix Q resulting from its QR decomposition is in this case an isometry, which determines $P_k|0\rangle$. This information can be completed at our best convenience to define the $M+1$ qubit gate P_k that is to be implemented on the quantum circuit.

In order to solve (18), we multiply both sides with the Hermitian conjugate to obtain a recursion relation

involving only the upper triangular matrices G_k , *i.e.*

Once the solution G_k has been calculated, we extract the P_k from

$$P_k |0\rangle = (\mathbb{1} \otimes G_{k-1})(\mathcal{R}_T |0\rangle)G_k^{-1}. \quad (20)$$

For $k < M$ a similar relation holds

$$P_k = (\mathbb{1} \otimes G_{k-1})(\mathcal{R}_T |0\rangle)H_k. \quad (21)$$

Recall that $G_{k < M-1}$ are not square matrices and hence do not have an inverse. However, there exists an upper rectangular matrix H_k satisfying $G_k H_k = \mathbb{1}$, which is thus sufficient for our purposes. The recursion relation (19) can be written as

$$\langle 0 | \mathcal{R}_T^\dagger (\mathbb{1} \otimes G_{k-1}^\dagger G_{k-1}) \mathcal{R}_T |0\rangle = G_k^\dagger G_k. \quad (22)$$

Although the dimensions of G_k vary in the first iterations, the product $G_k^\dagger G_k$ always defines a $2^M \times 2^M$ matrix. This renders the previous equation applicable to all iterations.

The protocol ends at the bottom-left cell

The correct normalization of the output Bethe state $|\Psi_M\rangle$ from the ABA requires one to suitably adjust the global factor ρ of the R matrix (7). If this is done, g will be a trivial phase. Alternatively, we might ignore the difficult issue of the finding the appropriate ρ for the desired eigenstate and just set $\rho = 1$. The output state from (12) will not be properly normalized, but the problem is simply solved by discarding the global factor g . We adopt this convention in the following. The previous relation (23) only determines the action of P_{N-1} on the state $|1 \dots 10\rangle$. This last unitary can be otherwise chosen freely.

We have thus obtained a deterministic quantum circuit for the preparation of BA eigenstates on N sites requiring only N qubits. The upper triangular structure

of G_k is key to the feasibility of our protocol. It implies the reduction of (19) to a nested system of equations. Substituting the solution of one equation into the next, we only need to care for one entry of G_k at a time. Moreover the inverse of a triangular matrix, required to obtain the unitaries P_k , is not expensive to calculate. The bottleneck of the procedure is the exponential growth in the number of equations with the number of magnons. Nevertheless, we have found that this is not prohibitive to explore cases of interest.

Two important comments on the QR decomposition should be added. The matrices Q and R are not fully determined but enjoy the gauge freedom

$$Q \rightarrow Q D^{-1}, \quad R \rightarrow D R, \quad (24)$$

where D is an arbitrary diagonal matrix containing complex phases. This freedom will be crucial below, when compiling the unitaries to elementary quantum gates. Additionally, the QR decomposition is compatible with the $U(1)$ symmetry of the XXZ model. Hence, all matrices G_k and P_k will conserve individually the number of excitations.

We end with a final remark. It has been shown that the BA can be interpreted in the language of tensor networks as a Matrix Product State (MPS) [26–28]. Our algorithm for the distillation of unitaries from the \mathcal{R}_T matrices is closely related to the transformation of an MPS into canonical form [29]. The tensors of a canonical MPS define isometries, and thus have a direct translation to a quantum circuit. The main difference with our approach lies in the elimination of the ancillary qubits, which renders the circuit deterministic. Hence the ABCs could prove relevant, not only for the preparation of eigenstates of integrable spin chains, but also for general MPS of low bond dimension. We note that the implementation of tensor-network states on a quantum computer has been addressed in [30–35].

B. One-magnon solution

We illustrate our method by explicitly deriving the circuit that constructs one-magnon states for the XXZ model. In order to study the properties of the P_k gates, we find it convenient to use the magnon quasi-momentum p instead of the rapidity λ as the basic variable. Indeed, the R matrix (7) has a simple expression in terms of s_1 and $s_2 = e^{ip}$. Besides, the integrability constrain (8) turns the parameter s_1 into a function of the quasi-momentum and the anisotropy.

The basic cell constructing one magnon solutions is composed of a single R matrix. In this case all the G_k matrices are 2×2 upper triangular. The preservation of $U(1)$ symmetry further forces them to be diagonal. We choose the following ansatz

$$G_k = \begin{pmatrix} 1 & 0 \\ 0 & s_1 c_k \end{pmatrix}. \quad (25)$$

The initial matrix G_0 defined in (13) is of this form with $c_0 = 1$. For $k > 0$, the gauge freedom of the QR decomposition allows us to set the c_k parameters to be real and positive. Equation (19) translates then into the recursion relation

$$c_k^2 = c_{k-1}^2 |s_2|^2 + 1, \quad (26)$$

for $k \geq 1$. Using the initial condition $c_0 = 1$, we arrive at the simple solution

$$c_k = \sqrt{k+1}. \quad (27)$$

where we have used that the quasi-momentum of the one magnon solutions must be real, implying that s_2 is a phase.

Substituting into (20) and completing the matrix, we obtain the two-qubit quantum gates

$$P_k = \begin{pmatrix} 1 & 0 & 0 & 0 \\ 0 & \frac{1}{\sqrt{k+1}} & -\sqrt{\frac{k}{k+1}} e^{-ip} & 0 \\ 0 & \sqrt{\frac{k}{k+1}} e^{ip} & \frac{1}{\sqrt{k+1}} & 0 \\ 0 & 0 & 0 & 1 \end{pmatrix}, \quad (28)$$

written with the convention

$$(P_k)_{i_1 i_2}^{j_1 j_2} = \begin{array}{c} j_2 \quad j_1 \\ | \\ \boxed{P_k} \\ | \\ i_2 \quad i_1 \end{array}. \quad (29)$$

We have ordered the input and output qubits from right to left instead of the customary left to right order, since this is better suited to the structure of the ABC. Indeed, with this convention the first two columns of (28) describe $P_k |0\rangle$. Both choices of order are related by a change of basis which, actually, leaves invariant the R -matrix (7).

One-magnon solutions are just plane waves. The anisotropy parametrizes the strength of interactions among magnons and it hence should have no influence on these configurations. Consequently, the unitaries P_k are independent of Δ . This is in contrast with the ABA circuit network (12), where every element depends on both s_1 and s_2 , or equivalently, on Δ and p . It is only the output of the complete circuit that builds the one-magnon states which is independent of the anisotropy. In our scheme, the local dependence on Δ is confined to the unphysical matrices G_k . Our construction offers an economic way of implementing plane waves on quantum hardware, with just nearest-neighbor connectivity among qubits. The special case $p = 0$ reproduces the optimal algorithm for obtaining the W state [42].

C. The XX model

The XX model, obtained when $\Delta = 0$, is the simplest member of the XXZ family. It describes a spinless free

fermion system via the Jordan-Wigner transformation. This was used in [24] to construct an efficient quantum circuit to prepare its eigenstates with a number of gates that is quadratic in the number of sites N . We will show that the ABC requires $\mathcal{O}(NM)$ gates, thus scaling linearly with the product of the number of sites and magnons.

We search for a decomposition of the unitaries P_k in terms of two-qubit quantum gates. In particular, we will use the phased F_{sim} gate [21] as the basic building block of our circuit, defined as

$$F = \begin{pmatrix} 1 & 0 & 0 & 0 \\ 0 & \cos \theta e^{i\alpha} & -\sin \theta e^{-i\beta} & 0 \\ 0 & \sin \theta e^{i\beta} & \cos \theta e^{-i\alpha} & 0 \\ 0 & 0 & 0 & 1 \end{pmatrix}. \quad (30)$$

This matrix is a $U(1)$ -symmetry-preserving generalization of the one-magnon unitaries (28). We use an ansatz in which the F gates reproduce the same contraction structure as the R matrices in the basic \mathcal{R}_T cell, *i.e.*

$$\begin{array}{c} | \\ \boxed{P_k} \\ | \end{array} = \begin{array}{c} | \\ \boxed{F_{M,k}} \\ | \end{array} \cdots \begin{array}{c} | \\ \boxed{F_{2,k}} \\ | \end{array} \begin{array}{c} | \\ \boxed{F_{1,k}} \\ | \end{array}. \quad (31)$$

In Appendix D we present the complete solution for two and three magnons in the XX model, including the closed-form of the matrices P_k . Furthermore, we verify the previous ansatz and analytically derive the parameters of the F gates. We have checked numerically that (31) holds up to six magnons. It also holds for the unitaries P_k with $k < M$, which act on a reduced number of qubits. Based on this evidence, we conjecture that it is valid in general.

In spite of the similar decompositions of the matrices P_k and \mathcal{R}_T , there is an important difference between them. Each R_j matrix in \mathcal{R}_T depends on a single magnon quasi-momentum p_j . On the contrary, the two-qubit gates $F_{j,k}$ contain information from all magnons down to position j , as seen in (D7)-(D9). Explicitly, the gate $F_{M,k}$ is a function of a single quasi-momentum p_M , while $F_{1,k}$ involves all of them.

The phase freedom shown in (24) is essential for (31) to hold. It is simple to see that the one-spin-down sector of P_k fixes completely this ansatz. The free phases affecting other symmetry sectors have then to be chosen appropriately for the so derived $F_{j,k}$ to describe the complete P_k . This choice has been implemented in the two and three magnon unitaries presented in Appendix D. Since G_k and P_k preserve the $U(1)$ symmetry, the one-spin-down sector can be determined independently from all others from the recursion relation (22). This implies that only $\frac{M(M+1)}{2}$ classical equations need to be solved. Hence our algorithm for the XX model is efficient both in its classical and quantum parts.

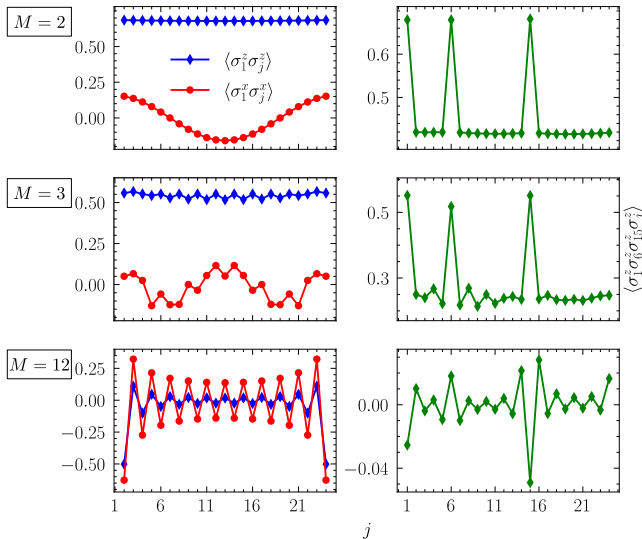


FIG. 3. Two-point and four-point correlators computed using the ABCs. Qubits are numbered from right to left, i.e. $j = 1$ indicates the rightmost qubit. From top to bottom, we simulate two excited states of the XXX and XXZ ($\Delta = 0.5$) models for $N = 24$ sites and $M = 2, 3$ magnons, respectively. Here, the roots of the Bethe equations are complex and take values $(-7.229 + 1.644i, -7.229 - 1.644i)$ and $(3.133 - 1.038i, -0.367, 3.133 + 1.038i)$. In the lowermost plot we show the simulation of the ground state of the XXZ model ($\Delta = 0.5$) for $N = 24$. The rapidities are real, with values $(-1.753, -1.031, -0.689, -0.451, -0.257, -0.084, 0.084, 0.257, 0.451, 0.689, 1.031, 1.753)$.

We have dropped the sub-index σ in M_k since in this case there is only one possible permutation, which interchanges λ and μ . The analytical expression is presented in Appendix F. Although all elements on the right-hand side of (40) depend on the anisotropy, their product does not. This implies that M_k is the same function of the magnon quasi-momenta for all members of the XXZ family. In consequence, a potential interpretation of (40) as a unitary version of the R matrix should be discarded. We must stress that the independence of the exchange matrices on the anisotropy does not hold for $M \geq 3$. These matrices are interesting objects in their own right, deserving further study.

V. NUMERICAL AND EXPERIMENTAL RESULTS

A. Simulation of correlator measurements

We performed numerical simulations to verify and illustrate our theoretical results, using the open-source library `Qibo` [47, 48]. We numerically solved the Bethe equations (2) and simulated the unitary circuits for two excited states of the XXX and XXZ ($\Delta = 0.5$) models for $N = 24$ qubits and $M = 2, 3$ magnons respectively,

and for the ground state of the XXZ model ($\Delta = 0.5$), for $N = 24$ qubits. We compared the resulting eigenstates with the simulated ABA states, finding a perfect agreement between the two. We then used these states to compute two-point and four-point correlation functions (as shown in Fig. 3) to illustrate the proposal of obtaining high-order correlators from BA eigenstates. The circuits were simulated in double precision using the `qibo` backend [49] on multi-threading CPU. They were directly obtained by computing the QR decompositions that are required to convert the ABA into a deterministic quantum circuit.

B. Plane waves on quantum hardware

We also implemented the circuit construction for plane wave states for system sizes $N = 6, 7, 8$ on the quantum computer *IBM_Montreal*. Once again, we explored the two site correlators from the prepared state (see Fig. 4).

As previously shown, the 2 qubit P_k unitary gates are simply phased *Fsim* gates when $M = 1$. These gates were decomposed into the IBM native gate set to be implemented on the hardware. The circuits used to prepare these states have total depths 47, 56 and 65 respectively. Each unitary gate involved 2 CNOT gates, leading to $2(N - 1)$ CNOT gates in total.

Current devices suffer from significant hardware noise. In order to obtain the best possible results it is necessary to use error mitigation which focuses on reducing the impact of noise rather than removing its effects completely. In this work we implemented three techniques: zero-noise extrapolation (ZNE) [50], Clifford data regression (CDR) [51] and variable noise Clifford data regression (vnCDR) [52]. We used the open source software package `Mitiq` [53] to execute these methods. For more details regarding the implementation of these techniques we refer the reader to Appendix G.

We benchmark the performance of each method by calculating an average relative error, defined as:

$$\langle \bar{O} \rangle_{Err} = \frac{\sum_j |\langle O_j \rangle_{exp} - \langle O_j \rangle_{exact}|}{\text{mean}(|\langle O_j \rangle_{exact}|)} \quad (41)$$

where O_j is some observable of interest and $\langle O_j \rangle_{exp}$ is the estimated value for that observable obtained experimentally with or without error mitigation. To simplify the comparison between mitigation techniques we average the above error metric across all the different observables and system sizes. We expect use this metric to reflect the overall performance of the mitigation methods while also taking into account the magnitude of the observables to mitigate. Furthermore, to simplify the presentation we omit the CDR mitigated results from our plots, we see that in general the performance is significantly better than ZNE but worse than vnCDR.

Error mitigation significantly improves the results obtained from the real device. We find that the average

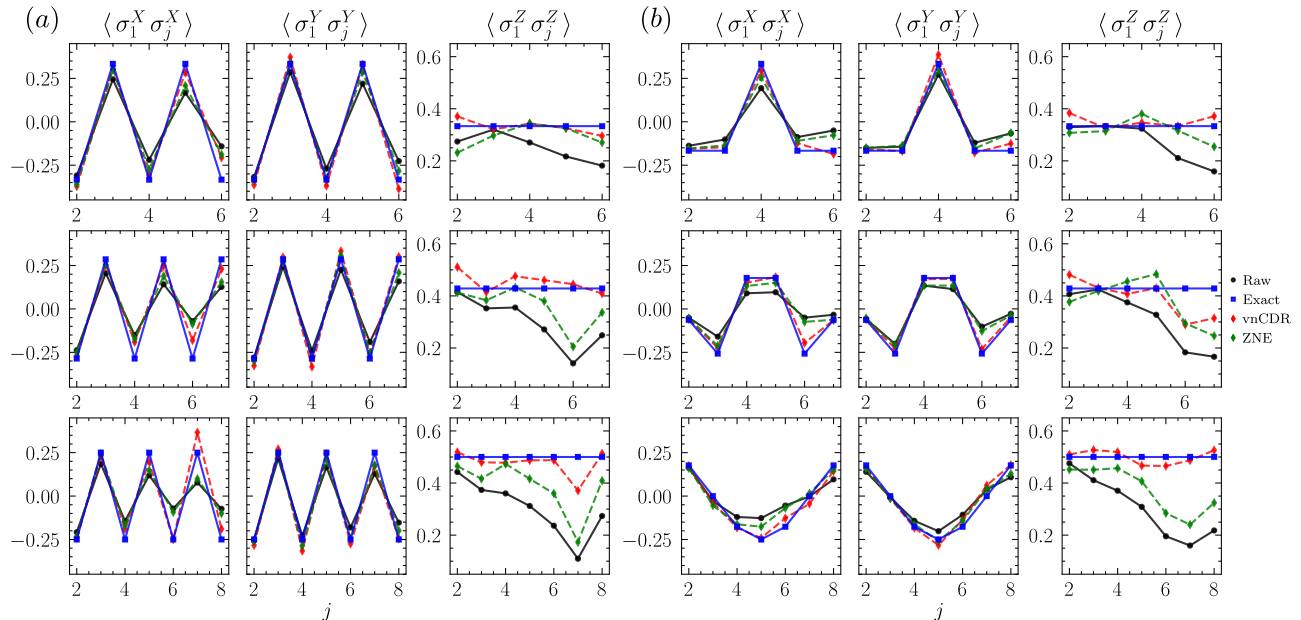
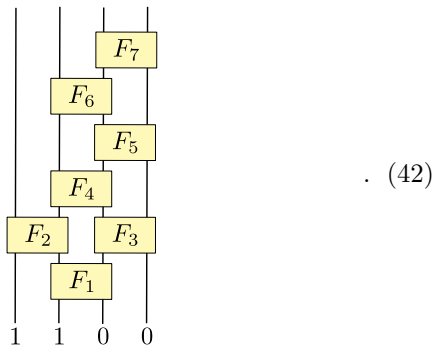


FIG. 4. Two-point correlators calculated using the quantum computer *IBM_Montreal*. Qubits are numbered from right to left, i.e. $j = 1$ indicates the rightmost qubit. From top to bottom, we simulate three plane waves with $N = 6, 7, 8$ sites. In (a) $p = \pi$ for all rows, in (b) $p = 4.189, 4.489, 5.498$, for each row from top to bottom respectively. Error mitigation is implemented with ZNE and vnCDR.

relative error is improved by factors of 1.57, 2.71 and 2.79 for ZNE, CDR and vnCDR respectively relative to the noisy results. As the observables become less local and the circuit depth increases, the quality of the raw and error mitigated results tends to decrease. This is particularly noticeable in the results obtained for the $\langle \sigma_1^Z \sigma_j^Z \rangle$ correlators. Clearly both vnCDR and ZNE tend to perform best in shallower, less noisy circuits although they still improve results for the deepest circuits explored here.

C. Two-magnon states on quantum hardware

In addition, we implement the circuits for two magnon states on current quantum hardware. We construct the ground state of the XX and XXZ models for 4 sites and an excited state of the XX model for 5 sites. The circuit for the ground state of the XXZ model consists of 7 F gates with an additional phase parameter, structured as follows:



We only need to determine the action of the last unitary P_{N-1} on the state $|110\rangle$ and this can be achieved with a single layer of F gates. This is a general property of all our Bethe circuits.

Once the F gates have been decomposed into the IBM native gate set the circuit to prepare these states have depths 40, 57 and 49 and involve 10, 16 and 14 CNOT gates respectively.

We evaluate the two-point correlators for these states across the chain, and mitigate the effect of hardware noise with ZNE and vnCDR (see Fig. 5). The average relative error (41) across all observables and system sizes is improved by factors of 1.71, 3.53 and 3.87 for ZNE, CDR and vnCDR. For two magnon states we explored smaller system sizes due to the increased scaling of depth with the number of qubits. We find that good agreement can be obtained between the exact and error mitigated observables, with vnCDR reducing the effect of noise the most.

Overall, these experiments show a proof of principle implementation of our approach for low numbers of magnons. Furthermore, they highlight the utility of error mitigation. In particular they show further evidence that learning based error mitigation is practically useful in reducing the effects of hardware noise. For larger scale implementations a combination of noise reduction and error mitigation techniques will be needed, which presents an exciting challenge for future experiments.

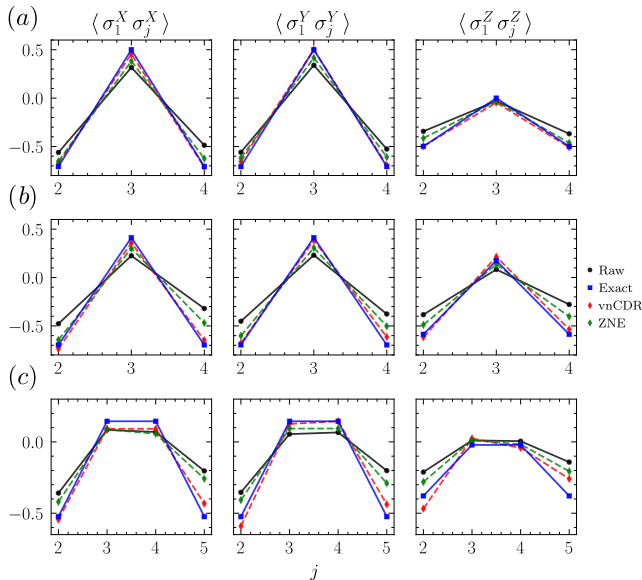


FIG. 5. Two-point correlators for several states with 2 magnons calculated using the quantum computers *IBM_Montreal* in (a) and (b) and *IBM_Mumbai* in (c). In (a) we prepare the ground state of the XX model for 4 sites. In (b) we prepare the ground state of the XXZ model for 4 sites and $\Delta = 0.5$. Finally, in (c) we prepare an excited state of the XX model with 2 magnons. The roots of the Bethe equations defining these states are, $(-0.561, 0.561)$, $(-0.574, 0.574)$ and $(-1.173, 0)$.

D. Yang-Baxter equation on quantum hardware

We have also verified the unitarised YB equation (37) on the cloud quantum computer *IBM_Cairo*, for the case $M = 2$ magnons in the XX model, given by

$$\begin{array}{c}
 \begin{array}{|c|} \hline F_{2,k}(\mu, \lambda) \\ \hline \end{array} \\
 \begin{array}{|c|} \hline F_{1,k}(\mu, \lambda) \\ \hline \end{array} \\
 \begin{array}{|c|} \hline M_k(\lambda, \mu) \\ \hline \end{array} \\
 \hline \\
 \begin{array}{|c|} \hline M_{k-1}(\lambda, \mu) \\ \hline \end{array} \\
 \begin{array}{|c|} \hline F_{2,k}(\lambda, \mu) \\ \hline \end{array} \\
 \begin{array}{|c|} \hline F_{1,k}(\lambda, \mu) \\ \hline \end{array} \\
 \hline \\
 \begin{array}{|c|} \hline 0 \\ \hline \end{array} \\
 \begin{array}{|c|} \hline 0 \\ \hline \end{array}
 \end{array} = \begin{array}{|c|} \hline F_{2,k}(\lambda, \mu) \\ \hline \end{array} \begin{array}{|c|} \hline F_{1,k}(\lambda, \mu) \\ \hline \end{array} . \quad (43)$$

We used state tomography to compute the density matrices associated with the right (ρ_r) and left (ρ_l) output states at both sides of (43) (see Table I). We computed these density matrices for each of the four possible initial input states, and we did so for the P_2 gate with Bethe roots $\lambda_1 = -1/\sqrt{3}$ and $\lambda_2 = 1/\sqrt{3}$. In order to compare ρ_r and ρ_l we determined the fidelity, given by

$$F = \left(\text{Tr} \sqrt{\sqrt{\rho_r} \rho_l \sqrt{\rho_r}} \right)^2 . \quad (44)$$

This heralds the first implementation of the YB equation on a quantum computer.

Initial state	Fidelity
$ 000\rangle$	0.969
$ 010\rangle$	0.964
$ 001\rangle$	0.962
$ 011\rangle$	0.950

TABLE I. Verification of the unitarised YB equation using the *IBM_Cairo* cloud quantum computer. The left column shows the initial state fed into (37), and the right column shows the fidelity between the output states at both sides of this equation.

VI. DISCUSSION

In this work, we have introduced a simple method to exactly prepare eigenstates of quantum integrable vertex models on programmable digital quantum computers. Our approach relies on using the QR decomposition as the main tool to bring the ABA to unitary form. In contrast to previous proposals, our method works for both real and complex roots of the Bethe equations and is deterministic. Both the circuit depth and gate complexity of our approach scale linearly with the number of qubits. However, we expect an exponential scaling in the number of magnons in general. This could appear in the time needed to bring the ABA to a unitary form and also in the decomposition of the unitary matrices to quantum gates.

Despite this, we find that with modest classical computational resources one can obtain a unitary circuit representation for interesting states. For the XX model, which can be mapped to free fermions, we find an efficient gate decomposition with polynomial classical effort. In particular, our approach produces quantum circuits that match the state-of-the-art $\mathcal{O}(N)$ depth of [21–23, 54].

Our algorithm opens up the possibility to prepare highly non-trivial ABA eigenstates on quantum computers. Foreseeable applications include using these states to study Hamiltonian quenches that may be inaccessible to classical methods. More generally, these states could be used as inputs to other quantum algorithms. For instance, it would be interesting to explore if they can be used to initialize variational quantum algorithms. Using such states may provide an initial state with sufficient overlap with the desired output for the optimization to be successful. This would combat the trainability issues of such approaches [55, 56]. Furthermore, our algorithm could be used to benchmark quantum hardware on strongly-correlated states whenever analytical solutions are known for some expectation values. This can be thought of as a type of application-oriented benchmark [57].

There remain many open questions that would be interesting to explore in future works. A clear next step will be to investigate the optimal strategy with which to compile the unitary gates P_k to improve the perfor-

mance for systems of many magnons [58, 59]. Extending our method to open boundary conditions and to other models, such as the Hubbard or Kondo models, is another clear research direction. Additionally, we want to stress that our approach can be used to represent an MPS as a deterministic quantum circuit, which would enable direct preparation of these states on a quantum computer.

Finally, it would be interesting to explore if the ABC can be used as a variational ansatz with which to solve the Bethe equations in future quantum devices. Using the ABC one could envision employing a variational approach to find the optimal parameters of the circuit and therefore solve the Bethe equations.

ACKNOWLEDGEMENTS

We acknowledge Luigi Amico, Marco Cerezo, Lukasz Cincio, Artur Garcia-Saez, Karen Hallberg, Hosho Katsura, Martín Larocca, José Ignacio Latorre, Rafael Nepomechie and Balázs Pozsgay for useful discussions. We thank the IBM Quantum team for making devices

available via the IBM Quantum Experience. The access to the IBM Quantum Experience has been provided by the CSIC IBM Q Hub. A.S. is supported by the Spanish Ministry of Science and Innovation under grant number SEV-2016-0597-19-4. M.H.G. was supported by “la Caixa” Foundation (ID 100010434), Grant No. LCF/BQ/DI19/11730056 and by the U.S. DOE, Office of Science, Office of Advanced Scientific Computing Research, under the Quantum Computing Application Teams program. D.G.M. is supported by project QuantumCAT (ref. 001- P-001644), co-funded by the Generalitat de Catalunya and the European Union Regional Development Fund within the ERDF Operational Program of Catalunya. This work has also been financed by the Grant PGC2018-095862-B-C21 funded by MCIN/AEI/10.13039/501100011033 and by “ERDF A way of making Europe”, by the Spanish Research Agency (Agencia Estatal de Investigación) through the Grant IFT Centro de Excelencia Severo Ochoa No CEX2020-001007-S, funded by MCIN/AEI/10.13039/501100011033, by the Madrid grant PGC2018-095862-B-C21, QUITEMAD+S2013/ICE-2801, and by the CSIC Research Platform on Quantum Technologies PTI-001.

-
- [1] Seth Lloyd, “Universal quantum simulators,” *Science* **273**, 1073–1078 (1996).
- [2] Rafael I. Nepomechie, “Bethe ansatz on a quantum computer?” (2021), [arXiv:2010.01609](https://arxiv.org/abs/2010.01609) [quant-ph].
- [3] John S. Van Dyke, George S. Barron, Nicholas J. Mayhall, Edwin Barnes, and Sophia E. Economou, “Preparing bethe ansatz eigenstates on a quantum computer,” *PRX Quantum* **2** (2021), 10.1103/prxquantum.2.040329.
- [4] John S Van Dyke, Edwin Barnes, Sophia E Economou, and Rafael I Nepomechie, “Preparing exact eigenstates of the open xxz chain on a quantum computer,” *Journal of Physics A: Mathematical and Theoretical* **55**, 055301 (2022).
- [5] Wen Li, Mert Okyay, and Rafael I. Nepomechie, “Bethe states on a quantum computer: success probability and correlation functions,” (2022), [arXiv:2201.03021](https://arxiv.org/abs/2201.03021) [quant-ph].
- [6] H. Bethe, “Zur theorie der metalle,” *Zeitschrift für Physik* **71**, 205–226 (1931).
- [7] V. E. Korepin, N. M. Bogoliubov, and A. G. Izergin, *Quantum Inverse Scattering Method and Correlation Functions*, Cambridge Monographs on Mathematical Physics (Cambridge University Press, 1993).
- [8] L. D. Faddeev, “How algebraic bethe ansatz works for integrable model,” (1996), [arXiv:hep-th/9605187](https://arxiv.org/abs/hep-th/9605187) [hep-th].
- [9] César Gómez, Martí Ruiz-Altaba, and Germán Sierra, *Quantum Groups in Two-Dimensional Physics*, 1st ed. (Cambridge University Press, 1996).
- [10] Balázs Pozsgay, “Excited state correlations of the finite heisenberg chain,” *Journal of Physics A: Mathematical and Theoretical* **50**, 074006 (2017).
- [11] Wen Wei Ho and Timothy H. Hsieh, “Efficient variational simulation of non-trivial quantum states,” *SciPost Physics* **6** (2019), 10.21468/scipostphys.6.3.029.
- [12] Carlos Bravo-Prieto, Josep Lumbresas-Zarapico, Luca Tagliacozzo, and José I. Latorre, “Scaling of variational quantum circuit depth for condensed matter systems,” *Quantum* **4**, 272 (2020).
- [13] Roeland Wiersema, Cunlu Zhou, Yvette de Sereville, Juan Felipe Carrasquilla, Yong Baek Kim, and Henry Yuen, “Exploring entanglement and optimization within the hamiltonian variational ansatz,” *PRX Quantum* **1** (2020), 10.1103/prxquantum.1.020319.
- [14] Manpreet Singh Jattana, Fengping Jin, Hans De Raedt, and Kristel Michielsen, “Assessment of the variational quantum eigensolver: application to the heisenberg model,” (2022), [arXiv:2201.05065](https://arxiv.org/abs/2201.05065) [quant-ph].
- [15] Jarrod R. McClean, Sergio Boixo, Vadim N. Smelyanskiy, Ryan Babbush, and Hartmut Neven, “Barren plateaus in quantum neural network training landscapes,” *Nature Communications* **9** (2018), 10.1038/s41467-018-07090-4.
- [16] M. Cerezo, Andrew Arrasmith, Ryan Babbush, Simon C. Benjamin, Suguru Endo, Keisuke Fujii, Jarrod R. McClean, Kosuke Mitarai, Xiao Yuan, Lukasz Cincio, and Patrick J. Coles, “Variational quantum algorithms,” *Nature Reviews Physics* **3**, 625–644 (2021).
- [17] Martín Larocca, Piotr Czarnik, Kunal Sharma, Gopikrishnan Muraleedharan, Patrick J. Coles, and M. Cerezo, “Diagnosing barren plateaus with tools from quantum optimal control,” (2021), [arXiv:2105.14377](https://arxiv.org/abs/2105.14377) [quant-ph].
- [18] Samson Wang, Enrico Fontana, M. Cerezo, Kunal Sharma, Akira Sone, Lukasz Cincio, and Patrick J. Coles, “Noise-induced barren plateaus in variational

- quantum algorithms,” *Nature Communications* **12** (2021), 10.1038/s41467-021-27045-6.
- [19] Gene H. Golub and Charles F. Van Loan, *Matrix computations*, 3rd ed., Johns Hopkins studies in the mathematical sciences (Johns Hopkins University Press, Baltimore, 1996).
- [20] Pieter W. Claeys, Jonah Herzog-Arbeitman, and Austen Lamacraft, “Correlations and commuting transfer matrices in integrable unitary circuits,” *SciPost Physics* **12** (2022), 10.21468/scipostphys.12.1.007.
- [21] Ian D. Kivlichan, Jarrod McClean, Nathan Wiebe, Craig Gidney, Alán Aspuru-Guzik, Garnet Kin-Lic Chan, and Ryan Babbush, “Quantum simulation of electronic structure with linear depth and connectivity,” *Physical Review Letters* **120** (2018), 10.1103/physrevlett.120.110501.
- [22] Zhang Jiang, Kevin J. Sung, Kostyantyn Kechedzhi, Vadim N. Smelyanskiy, and Sergio Boixo, “Quantum algorithms to simulate many-body physics of correlated fermions,” *Physical Review Applied* **9** (2018), 10.1103/physrevapplied.9.044036.
- [23] Frank Arute, Kunal Arya, Ryan Babbush, Dave Bacon, Joseph C. Bardin, *et al.*, “Observation of separated dynamics of charge and spin in the fermi-hubbard model,” (2020), [arXiv:2010.07965 \[quant-ph\]](https://arxiv.org/abs/2010.07965).
- [24] Frank Verstraete, J. Ignacio Cirac, and José I. Latorre, “Quantum circuits for strongly correlated quantum systems,” *Physical Review A* **79** (2009), 10.1103/physreva.79.032316.
- [25] Alba Cervera-Lierta, “Exact Ising model simulation on a quantum computer,” *Quantum* **2**, 114 (2018).
- [26] Francisco C Alcaraz and Matheus J Lazo, “The bethe ansatz as a matrix product ansatz,” *Journal of Physics A: Mathematical and General* **37**, L1–L7 (2003).
- [27] Hoshio Katsura and Isao Maruyama, “Derivation of the matrix product ansatz for the heisenberg chain from the algebraic bethe ansatz,” *Journal of Physics A: Mathematical and Theoretical* **43**, 175003 (2010).
- [28] V. Murg, V. E. Korepin, and F. Verstraete, “Algebraic bethe ansatz and tensor networks,” *Physical Review B* **86** (2012), 10.1103/physrevb.86.045125.
- [29] D. Perez-Garcia, F. Verstraete, M. M. Wolf, and J. I. Cirac, “Matrix product state representations,” (2007), [arXiv:quant-ph/0608197 \[quant-ph\]](https://arxiv.org/abs/quant-ph/0608197).
- [30] Shi-Ju Ran, “Encoding of matrix product states into quantum circuits of one- and two-qubit gates,” *Phys. Rev. A* **101**, 032310 (2020).
- [31] Adam Smith, Bernhard Jobst, Andrew G. Green, and Frank Pollmann, “Crossing a topological phase transition with a quantum computer,” (2021), [arXiv:1910.05351 \[cond-mat.str-el\]](https://arxiv.org/abs/1910.05351).
- [32] Sheng-Hsuan Lin, Rohit Dilip, Andrew G. Green, Adam Smith, and Frank Pollmann, “Real- and imaginary-time evolution with compressed quantum circuits,” *PRX Quantum* **2**, 010342 (2021).
- [33] F. Barratt, James Dborin, Matthias Bal, Vid Stojevic, Frank Pollmann, and A. G. Green, “Parallel quantum simulation of large systems on small nisc computers,” *npj Quantum Information* **7** (2021), 10.1038/s41534-021-00420-3.
- [34] Michael Foss-Feig, David Hayes, Joan M. Dreiling, Caroline Figgatt, John P. Gaebler, Steven A. Moses, Juan M. Pino, and Andrew C. Potter, “Holographic quantum algorithms for simulating correlated spin systems,” *Physical Review Research* **3** (2021), 10.1103/physrevresearch.3.033002.
- [35] Reza Haghshenas, Johnnie Gray, Andrew C. Potter, and Garnet Kin-Lic Chan, “The variational power of quantum circuit tensor networks,” (2021), [arXiv:2107.01307 \[quant-ph\]](https://arxiv.org/abs/2107.01307).
- [36] Rodney J. Baxter, *Exactly solved models in statistical mechanics*, dover ed ed. (Dover Publications, Mineola, N.Y., 2007) oCLC: ocn154799434.
- [37] Bill Sutherland, *Beautiful Models: 70 Years of Exactly Solved Quantum Many-Body Problems* (WORLD SCIENTIFIC, 2004).
- [38] G. Mussardo, *Statistical field theory: an introduction to exactly solved models in statistical physics*, Oxford graduate texts (Oxford University Press, Oxford ; New York, 2010) oCLC: ocn359673689.
- [39] Édouard Brézin and Jean Zinn-Justin, *Champs, cordes et phénomènes critiques: les Houches, session XLIX, 28 Juin-5 Août 1988* (North-Holland, Amsterdam Oxford New York, 1990).
- [40] Thierry Giamarchi, *Quantum physics in one dimension*, The international series of monographs on physics No. 121 (Clarendon ; Oxford University Press, Oxford : New York, 2004) oCLC: ocm52784724.
- [41] Dave Wecker, Matthew B. Hastings, Nathan Wiebe, Bryan K. Clark, Chetan Nayak, and Matthias Troyer, “Solving strongly correlated electron models on a quantum computer,” *Phys. Rev. A* **92**, 062318 (2015).
- [42] Diogo Cruz, Romain Fournier, Fabien Gremion, Alix Jeannerot, Kenichi Komagata, Tara Tosic, Jarla Thiesbrummel, Chun Lam Chan, Nicolas Macris, Marc-André Dupertuis, and *et al.*, “Efficient quantum algorithms for ghz and w states, and implementation on the ibm quantum computer,” *Advanced Quantum Technologies* **2**, 1900015 (2019).
- [43] Sumeet Khatri, Ryan LaRose, Alexander Poremba, Lukasz Cincio, Andrew T. Sornborger, and Patrick J. Coles, “Quantum-assisted quantum compiling,” *Quantum* **3**, 140 (2019).
- [44] Kunal Sharma, Sumeet Khatri, M Cerezo, and Patrick J Coles, “Noise resilience of variational quantum compiling,” *New Journal of Physics* **22**, 043006 (2020).
- [45] Efehan Kökcü, Thomas Steckmann, J. K. Freericks, Eugene F. Dumitrescu, and Alexander F. Kemper, “Fixed depth hamiltonian simulation via cartan decomposition,” (2021), [arXiv:2104.00728 \[quant-ph\]](https://arxiv.org/abs/2104.00728).
- [46] Alexander B Zamolodchikov and Alexey B Zamolodchikov, “Factorized s-matrices in two dimensions as the exact solutions of certain relativistic quantum field theory models,” *Annals of Physics* **120**, 253–291 (1979).
- [47] Stavros Efthymiou, Sergi Ramos-Calderer, Carlos Bravo-Prieto, Adrián Pérez-Salinas, Diego García-Martín, Artur Garcia-Saez, José Ignacio Latorre, and Stefano Carrazza, “Qibo: a framework for quantum simulation with hardware acceleration,” *Quantum Science and Technology* **7**, 015018 (2021).
- [48] Stavros Efthymiou, Stefano Carrazza, AdrianPerezSalinas, Sergi Ramos, Carlos Bravo-Prieto, Diego García-Martín, Nicole Zattarin, Marco Lazzarin, Paul, Andrea Pasquale, Javier Serrano, and atomicprinter, “qiboteam/qibo: Qibo 0.1.7-rc1,” (2021).
- [49] Stavros Efthymiou, Stefano Carrazza, Marco Lazzarin, and Andrea Pasquale, “qiboteam/qibojit: qibojit 0.0.4,” (2022).

- [50] Kristan Temme, Sergey Bravyi, and Jay M. Gambetta, “Error mitigation for short-depth quantum circuits,” *Physical Review Letters* **119** (2017), [10.1103/physrevlett.119.180509](https://doi.org/10.1103/physrevlett.119.180509).
- [51] Piotr Czarnik, Andrew Arrasmith, Patrick J. Coles, and Lukasz Cincio, “Error mitigation with clifford quantum-circuit data,” *Quantum* **5**, 592 (2021).
- [52] Angus Lowe, Max Hunter Gordon, Piotr Czarnik, Andrew Arrasmith, Patrick J. Coles, and Lukasz Cincio, “Unified approach to data-driven quantum error mitigation,” *Physical Review Research* **3** (2021), [10.1103/physrevresearch.3.033098](https://doi.org/10.1103/physrevresearch.3.033098).
- [53] Ryan LaRose, Andrea Mari, Sarah Kaiser, Peter J. Karalekas, Andre A. Alves, Piotr Czarnik, Mohamed El Mandouh, Max H. Gordon, Yousef Hindy, Aaron Robertson, Purva Thakre, Nathan Shammah, and William J. Zeng, “Mitiq: A software package for error mitigation on noisy quantum computers,” (2021), [arXiv:2009.04417 \[quant-ph\]](https://arxiv.org/abs/2009.04417).
- [54] Efehan Kökcü, Daan Camps, Lindsay Bassman, James K. Freericks, Wibe A. de Jong, Roel Van Beeumen, and Alexander F. Kemper, “Algebraic compression of quantum circuits for hamiltonian evolution,” (2021), [arXiv:2108.03282 \[quant-ph\]](https://arxiv.org/abs/2108.03282).
- [55] Edward Grant, Leonard Wossnig, Mateusz Ostaszewski, and Marcello Benedetti, “An initialization strategy for addressing barren plateaus in parametrized quantum circuits,” *Quantum* **3**, 214 (2019).
- [56] M. Cerezo, Akira Sone, Tyler Volkoff, Lukasz Cincio, and Patrick J. Coles, “Cost function dependent barren plateaus in shallow parametrized quantum circuits,” *Nature Communications* **12** (2021), [10.1038/s41467-021-21728-w](https://doi.org/10.1038/s41467-021-21728-w).
- [57] Thomas Lubinski, Sonika Johri, Paul Varosy, Jeremiah Coleman, Luning Zhao, Jason Necaie, Charles H. Baldwin, Karl Mayer, and Timothy Proctor, “Application-oriented performance benchmarks for quantum computing,” (2021), [arXiv:2110.03137 \[quant-ph\]](https://arxiv.org/abs/2110.03137).
- [58] Bobak Toussi Kiani, Seth Lloyd, and Reevu Maity, “Learning unitaries by gradient descent,” (2020), [arXiv:2001.11897 \[quant-ph\]](https://arxiv.org/abs/2001.11897).
- [59] Martin Larocca, Nathan Ju, Diego García-Martín, Patrick J. Coles, and M. Cerezo, “Theory of over-parametrization in quantum neural networks,” (2021), [arXiv:2109.11676 \[quant-ph\]](https://arxiv.org/abs/2109.11676).
- [60] Alejandro Sopena, Max Hunter Gordon, Germán Sierra, and Esperanza López, “Simulating quench dynamics on a digital quantum computer with data-driven error mitigation,” *Quantum Science and Technology* **6**, 045003 (2021).
- [61] Andre He, Benjamin Nachman, Wibe A. de Jong, and Christian W. Bauer, “Zero-noise extrapolation for quantum-gate error mitigation with identity insertions,” *Physical Review A* **102** (2020), [10.1103/physreva.102.012426](https://doi.org/10.1103/physreva.102.012426).
- [62] Lorenza Viola and Seth Lloyd, “Dynamical suppression of decoherence in two-state quantum systems,” *Physical Review A* **58**, 2733–2744 (1998).
- [63] Youngseok Kim, Christopher J. Wood, Theodore J. Yoder, Seth T. Merkel, Jay M. Gambetta, Kristan Temme, and Abhinav Kandala, “Scalable error mitigation for noisy quantum circuits produces competitive expectation values,” (2021), [arXiv:2108.09197 \[quant-ph\]](https://arxiv.org/abs/2108.09197).

Appendix A: Non-unitarity of the R matrices

We show here that the R matrices (7) appearing in the Algebraic Bethe Ansatz (ABA) are not unitary in general. We start with

$$RR^\dagger = |\rho|^2 \begin{pmatrix} 1 & 0 & 0 & 0 \\ 0 & |s_1|^2 + |s_2|^2 & s_1 s_2^* + s_2 s_1^* & 0 \\ 0 & s_1 s_2^* + s_2 s_1^* & |s_1|^2 + |s_2|^2 & 0 \\ 0 & 0 & 0 & 1 \end{pmatrix}, \quad (\text{A1})$$

where $*$ denotes the complex conjugate. In order for R to be unitary, the following conditions must be satisfied,

$$\begin{aligned} |\rho|^2 &= 1, \\ |s_1|^2 + |s_2|^2 &= 1, \\ s_1 s_2^* + s_2 s_1^* &= 0. \end{aligned} \quad (\text{A2})$$

After some straightforward algebra, the last two conditions are seen to imply

$$\text{Im } \lambda = 1 + \frac{2\pi n}{\gamma}, \quad (\text{A3})$$

with n an integer. However, in general the parameters λ that solve the Bethe equations do not satisfy this requirement.

Appendix B: The monodromy and transfer matrices

In the main text we have used a matrix $R_{12} : \mathcal{H}_1 \otimes \mathcal{H}_2 \rightarrow \mathcal{H}_2 \otimes \mathcal{H}_1$, where \mathcal{H}_1 and \mathcal{H}_2 are the vector space $\mathbb{C}^{\otimes 2}$. To define a transfer matrix it is customary to employ a matrix $\mathcal{R}_{12} : \mathcal{H}_1 \otimes \mathcal{H}_2 \rightarrow \mathcal{H}_1 \otimes \mathcal{H}_2$, that is related to R_{12} by a permutation P_{12} ,

$$\mathcal{R}_{12} = P_{12} R_{12}, \quad (\text{B1})$$

that reads in components

$$\mathcal{R}_{i_1 i_2}^{j_1 j_2} = R_{i_1 i_2}^{j_2 j_1} = \begin{array}{c} j_2 \\ \boxed{R} \\ i_2 \end{array} \begin{array}{c} j_1 \\ \text{---} \\ i_1 \end{array}. \quad (\text{B2})$$

The YB equation for the matrix $R(\lambda)$, given in (34), can be expressed in terms of $\mathcal{R}(\lambda)$ as

$$\mathcal{R}_{12}(\lambda - \mu) \mathcal{R}_{13}(\lambda) \mathcal{R}_{23}(\mu) = \mathcal{R}_{23}(\mu) \mathcal{R}_{13}(\lambda) \mathcal{R}_{12}(\lambda - \mu). \quad (\text{B3})$$

The monodromy matrix $T(\lambda)$ is a linear map from $\mathcal{H}_a \otimes \mathcal{H}_1 \otimes \dots \otimes \mathcal{H}_N$ to itself, where \mathcal{H}_a is an auxiliary space and \mathcal{H}_j the local quantum spaces ($j = 1, \dots, N$). Its definition is [9]

$$T(\lambda) = \mathcal{R}_{aN}(\lambda) \mathcal{R}_{aN-1}(\lambda) \dots \mathcal{R}_{a2}(\lambda) \mathcal{R}_{a1}(\lambda). \quad (\text{B4})$$

where

$$\mathcal{R}_{aj}(u) : \mathcal{H}_a \otimes \mathcal{H}_j \rightarrow \mathcal{H}_a \otimes \mathcal{H}_j, \quad j = 1, \dots, N. \quad (\text{B5})$$

Equation (B4) reads in components

$$(T_a^b)_{i_1, \dots, i_N}^{j_1, \dots, j_N} = \sum_{a_1, \dots, a_{N-1}} \mathcal{R}_{a_{N-1} i_N}^{b j_N} \dots \mathcal{R}_{a_1 i_2}^{a_2 j_2} \mathcal{R}_{a_1 i_1}^{a_1 j_1}. \quad (\text{B6})$$

Notice that the contraction of the matrices \mathcal{R}_{aj} in the auxiliary space follows the rule $(XY)_c^a = X_b^a Y_c^b$, so that upper and lower indices correspond to row and column indices respectively. For the XXZ model we are considering $T(\lambda)$ is the 2×2 operator matrix given in (5)

$$T(\lambda) = \begin{pmatrix} T_0^0 & T_1^0 \\ T_0^1 & T_1^1 \end{pmatrix} = \begin{pmatrix} A & B \\ C & D \end{pmatrix}. \quad (\text{B7})$$

Equation (B6) can be given the tensor network notation by simply permutating the upper indices of the matrices \mathcal{R} ,

$$(\mathcal{T}_a^b)_{i_1, \dots, i_N}^{j_1, \dots, j_N} = \sum_{a_1, \dots, a_{N-1}} R_{a_{N-1} i_N}^{j_N b} \dots R_{a_1 i_2}^{j_2 a_2} R_{a_1 i_1}^{j_1 a_1}. \quad (\text{B8})$$

whose graphical representation is

$$\begin{array}{c} j_1 \quad j_2 \quad \dots \quad j_{N-1} \quad j_N \\ \boxed{R} \text{---} \boxed{R} \text{---} \dots \text{---} \boxed{R} \text{---} \boxed{R} \\ i_1 \quad i_2 \quad \dots \quad i_{N-1} \quad i_N \end{array} \begin{array}{c} a \\ \text{---} \\ b \end{array}. \quad (\text{B9})$$

The case $a = 1$ and $b = 0$ reproduces (4) giving the operator $B(\lambda)$. Finally, the transfer matrix is defined as the trace of the monodromy matrix (B7) in the auxiliary space which yields

$$t(\lambda) = \sum_{a=0,1} T_a^a(\lambda) = A + D, \quad (\text{B10})$$

that coincides with (6).

Appendix C: General solution for two magnons

The transformation of the ABA into a quantum circuit can be carried out analytically for the case of two magnons and for any number of sites N .

The \mathcal{R}_T basic cell is

$$\begin{array}{c} \boxed{\mathcal{R}_T} \\ 0 \end{array} = \begin{array}{c} \boxed{R_2} \\ | \\ \boxed{R_1} \\ 0 \end{array}, \quad (\text{C1})$$

with R_1 and R_2 parametrized by $r_{1,2}$ and $s_{1,2}$ respectively. The matrix G_0 (13), which defines the starting point of our algorithm, is given by

$$G_0 = \begin{pmatrix} 1 & 0 & 0 & 0 \\ 0 & s_1 & r_1 s_2 & 0 \end{pmatrix}. \quad (\text{C2})$$

From now on, we follow the right to left ordering of qubits explained in (29). Notice that this is opposite to

the customary left to right order used in Appendix B. Namely

$$(G_0)_{i_1 i_2}^j = \begin{array}{c} j \quad 0 \quad 0 \\ | \quad | \quad | \\ \text{---} \mathcal{R}_T \text{---} \\ | \quad | \quad | \\ i_2 \quad i_1 \quad 0 \end{array} . \quad (\text{C3})$$

When writing down the entries of an ABC matrix, we will always adopt this convention. Substituting into the recursion relations (22), we find

$$G_k = \begin{pmatrix} 1 & 0 & 0 & 0 \\ 0 & c_k s_1 & c_k r_1 \left(s_2 + \frac{f_k (s_1^2 + (r_2 - s_2) s_2) s_2^*}{c_k^2} \right) & 0 \\ 0 & 0 & \frac{-d_k r_1 (s_1^2 + (r_2 - s_2) s_2)}{c_k} & 0 \\ 0 & 0 & 0 & -e_k r_1 s_1 (1 + r_2 s_2) \end{pmatrix}, \quad (\text{C4})$$

for $k \geq 1$. The coefficients c_k , d_k and e_k are assumed to be real and positive using the gauge freedom (24). The new coefficients satisfy

$$c_k^2 = c_{k-1}^2 |s_2|^2 + 1, \quad (\text{C5})$$

$$f_k = f_{k-1} r_2 s_2^* + c_{k-1}^2, \quad (\text{C6})$$

$$c_{k-1}^2 d_k^2 = c_k^2 d_{k-1}^2 |r_2|^2 + |f_k|^2, \quad (\text{C7})$$

while e_k is given by

$$e_k^2 = d_k^2 - \frac{2\Delta}{|1+r_2 s_2|^2} \left[(d_k^2 - \bar{e}_k^2) (1+r_2 s_2) s_2^* + (d_k^2 - \bar{e}_k^{*2}) (1+r_2 s_2)^* s_2 \right] + \frac{4\Delta^2 |s_2 r_2|^2}{|1+r_2 s_2|^2} d_{k-1}^2, \quad (\text{C8})$$

with

$$\bar{e}_k^2 = \bar{e}_{k-1}^2 |r_2 s_2|^2 + f_k. \quad (\text{C9})$$

The initial conditions for these equations are

$$c_0 = 1, \quad f_0 = d_0 = e_0 = 0. \quad (\text{C10})$$

We obtain the first, 2-qubit unitary of the circuit from equation (21)

$$P_1 = \begin{pmatrix} 1 & 0 & 0 & 0 \\ 0 & \frac{1}{c_1} & \frac{s_2^*}{c_1} & 0 \\ 0 & \frac{s_2}{c_1} & \frac{-1}{c_1} & 0 \\ 0 & 0 & 0 & 1 \end{pmatrix}. \quad (\text{C11})$$

Equation (20) determines the action of 3-qubit unitaries

$P_{k>1}$ on the state $|0\rangle$ to be

$$P_k |0\rangle = \begin{pmatrix} 1 & 0 & 0 & 0 \\ 0 & \frac{1}{c_k} & \frac{f_k s_2^*}{c_k d_k} & 0 \\ 0 & \frac{c_{k-1} s_2}{c_k} & \frac{-f_k}{c_{k-1} c_k d_k} & 0 \\ 0 & 0 & 0 & \frac{-1}{c_{k-1} e_k} \left(f_k - \frac{2\Delta r_2}{1+r_2 s_2} |s_2|^2 f_{k-1} \right) \\ 0 & 0 & \frac{c_k d_{k-1} r_2}{c_{k-1} d_k} & 0 \\ 0 & 0 & 0 & \frac{d_{k-1} r_2}{c_{k-1} e_k} \left(1 - \frac{2\Delta s_2}{1+r_2 s_2} \right) \\ 0 & 0 & 0 & \frac{e_{k-1} r_2 s_2}{e_k} \\ 0 & 0 & 0 & 0 \end{pmatrix}. \quad (\text{C12})$$

The recursion relation (C5) defining the coefficients c_k is easily solved

$$c_k = \sqrt{1 + |s_2|^2 + \dots + |s_2|^{2k}}. \quad (\text{C13})$$

Recalling that s_2 is just a phase for one-magnon solutions, we obtain that the first columns of G_k and $P_k |0\rangle$ for two magnons contain the one-magnon solution (25) and the corresponding $P_k |0\rangle$ part of (28).

Appendix D: The XX model

The XX model is obtained when $\Delta = 0$. It is a free system and thus implies drastic simplifications with respect to the general XXZ model. The two magnon solution (C12) reduces in the XX model to

$$P_k |0\rangle = \begin{pmatrix} 1 & 0 & 0 & 0 \\ 0 & \frac{1}{c_k} & \frac{f_k s_2^*}{c_k d_k} & 0 \\ 0 & \frac{c_{k-1} s_2}{c_k} & \frac{-f_k}{c_{k-1} c_k d_k} & 0 \\ 0 & 0 & 0 & \frac{-f_k}{c_{k-1} d_k} \\ 0 & 0 & \frac{r_2 c_k d_{k-1}}{c_{k-1} d_k} & 0 \\ 0 & 0 & 0 & \frac{d_{k-1} r_2}{c_{k-1} d_k} \\ 0 & 0 & 0 & \frac{r_2 s_2 d_{k-1}}{d_k} \\ 0 & 0 & 0 & 0 \end{pmatrix}. \quad (\text{D1})$$

We have also derived the explicit three-magnon solution. The \mathcal{R}_T basic cell is now

$$\begin{array}{c} \mathcal{R}_T \\ | \quad | \quad | \\ \text{---} \text{---} \text{---} \\ | \quad | \quad | \\ 0 \end{array} = \begin{array}{c} R_3 \\ | \quad | \quad | \\ \text{---} \text{---} \text{---} \\ | \quad | \quad | \\ R_2 \\ | \quad | \quad | \\ \text{---} \text{---} \text{---} \\ | \quad | \quad | \\ R_1 \\ | \quad | \quad | \\ \text{---} \text{---} \text{---} \\ | \quad | \quad | \\ 0 \end{array}, \quad (\text{D2})$$

with R_1 , R_2 and R_3 parametrized by $t_{1,2}$, $r_{1,2}$ and $s_{1,2}$ respectively. We will just sketch the first iterations. The initial matrix G_0 (13) has now dimension 2×8 . The first step (14) results in a 4×8 non-unitary G_1 and the

4×4 gate P_1 (C11). The second iteration leads to G_2 and P_2 both of dimension 8×8 . From then on each

iteration distill a four qubit unitary, whose action on the rightmost $|0\rangle$ is

$$P_k|0\rangle = \begin{pmatrix} 1 & 0 & 0 & 0 & 0 & 0 & 0 & 0 \\ 0 & \frac{1}{c_k} & \frac{f_k s_2^*}{c_k d_k} & 0 & \frac{h_k s_2^* r_2^*}{d_k g_k} & 0 & 0 & 0 \\ 0 & \frac{c_{k-1} s_2}{c_k} & \frac{-f_k}{c_{k-1} c_k d_k} & 0 & \frac{-h_k r_2^*}{c_{k-1} d_k g_k} & 0 & 0 & 0 \\ 0 & 0 & 0 & \frac{-f_k}{c_{k-1} d_k} & 0 & \frac{-c_k h_k r_2^*}{c_{k-1} d_k g_k} & 0 & 0 \\ 0 & 0 & \frac{c_k d_{k-1} r_2}{c_{k-1} d_k} & 0 & \frac{-h_k f_k^*}{c_{k-1} d_{k-1} d_k g_k} & 0 & 0 & 0 \\ 0 & 0 & 0 & \frac{d_{k-1} r_2}{c_{k-1} d_k} & 0 & \frac{-h_k f_k^*}{c_{k-1} d_{k-1} c_k d_k g_k} & \frac{-c_{k-1} h_k s_2^*}{d_{k-1} c_k g_k} & 0 \\ 0 & 0 & 0 & \frac{d_{k-1} s_2 r_2}{d_k} & 0 & \frac{-h_k f_k^* s_2}{d_{k-1} c_k d_k g_k} & \frac{h_k}{d_{k-1} c_k g_k} & 0 \\ 0 & 0 & 0 & 0 & 0 & 0 & 0 & \frac{h_k}{d_{k-1} g_k} \\ 0 & 0 & 0 & 0 & \frac{d_k g_{k-1} t_2}{d_{k-1} g_k} & 0 & 0 & 0 \\ 0 & 0 & 0 & 0 & 0 & \frac{d_k g_{k-1} t_2}{d_{k-1} c_k g_k} & \frac{f_k g_{k-1} s_2^* t_2}{d_{k-1} c_k g_k} & 0 \\ 0 & 0 & 0 & 0 & 0 & \frac{c_{k-1} d_k g_{k-1} s_2 t_2}{d_{k-1} c_k g_k} & \frac{-f_k g_{k-1} t_2}{c_{k-1} d_{k-1} c_k g_k} & 0 \\ 0 & 0 & 0 & 0 & 0 & 0 & 0 & \frac{-f_k g_{k-1} t_2}{c_{k-1} d_{k-1} g_k} \\ 0 & 0 & 0 & 0 & 0 & 0 & \frac{c_k g_{k-1} r_2 t_2}{c_{k-1} g_k} & 0 \\ 0 & 0 & 0 & 0 & 0 & 0 & 0 & \frac{g_{k-1} r_2 t_2}{c_{k-1} g_k} \\ 0 & 0 & 0 & 0 & 0 & 0 & 0 & \frac{g_{k-1} s_2 r_2 t_2}{g_k} \\ 0 & 0 & 0 & 0 & 0 & 0 & 0 & 0 \end{pmatrix} \quad (D3)$$

The first four rows reproduce the two magnon solution (D1). The coefficients c_k , f_k and d_k are determined by (C5)-(C7), with the initial conditions (C10). The new coefficients h_k and g_k are determined by the recursion relations

$$h_k f_{k-1} = h_{k-1} f_k t_2 r_2^* + d_{k-1}^2 B_k, \quad (D4)$$

$$B_k = B_{k-1} t_2 s_2^* + f_{k-1}, \quad (D5)$$

$$d_{k-1} g_k^2 = |h_k|^2 + d_k^2 g_{k-1}^2 |t_2|^2, \quad (D6)$$

with g_k real and positive. The initial conditions for these equations are contained in G_1 . The simplicity of the XX model leads to the efficient decomposition of the unitaries P_k in terms of a single layer of *Fsim* gates. It is straightforward to check that the previous two magnon and three magnon matrices verify the ansatz in (31). The parameters (30) describing the corresponding gates $F_{j,k}$ are

$$a_{M,k} = \frac{1}{c_k}, \quad b_{M,k} = \frac{c_{k-1} s_2}{c_k}, \quad (D7)$$

$$a_{M-1,k} = -\frac{f_k}{c_{k-1} d_k}, \quad b_{M-1,k} = \frac{c_k d_{k-1} r_2}{c_{k-1} d_k}, \quad (D8)$$

$$a_{M-2,k} = \frac{h_k}{d_{k-1} g_k}, \quad b_{M-2,k} = \frac{d_k g_{k-1} t_2}{d_{k-1} g_k}, \quad (D9)$$

with $a = \cos \theta e^{i\alpha}$ and $b = \sin \theta e^{i\beta}$. For $M = 2$, only (D7) and (D8) are relevant.

Appendix E: Example of \mathcal{R}_σ with 3 magnons

The matrix \mathcal{R}_σ appearing in (35) is the essential element for the derivation of the unitary version of the YB equation. We present here an example of this matrix for a permutation involving three magnons. We assign the following rapidities to the R matrices in the basic cell (D2),

$$R_3 = R(\lambda), \quad R_2 = R(\mu), \quad R_1 = R(\nu), \quad (E1)$$

and consider the permutation $\sigma(\lambda, \mu, \nu) = (\nu, \mu, \lambda)$. Using the YB equation (34), this exchange is achieved by

$$\mathcal{R}_\sigma = \begin{array}{c} \text{---} \\ | \\ | \\ | \\ \text{---} \end{array} \begin{array}{c} R(\mu-\nu) \\ R(\lambda-\nu) \\ R(\lambda-\mu) \end{array} \begin{array}{c} \text{---} \\ | \\ | \\ | \\ \text{---} \end{array} \quad (E2)$$

